Polyhedron 31 (2012) 738–747

Contents lists available at SciVerse ScienceDirect

Polyhedron

journal homepage: www.elsevier.com/locate/poly

# Synthesis and structural characterization of organotin(IV) carboxylates based on different heterocyclic substituents

Wen-Qian Geng [a,d], Hong-Ping Zhou [a,*], Long-Huai Cheng [a], Fu-Ying Hao [a], Guo-Yi Xu [a], Fei-Xia Zhou [a], Zhi-Peng Yu [a], Zheng Zheng [a], Jian-Qing Wang [a], Jie-Ying Wu [a], Yu-Peng Tian [a,b,c,*]

[a] Department of Chemistry, Anhui University, Key Laboratory of Functional Inorganic Materials Chemistry of Anhui Province, 230039 Hefei, PR China
[b] State Key Laboratory of Coordination Chemistry, Nanjing University, 210093 Nanjing, PR China
[c] State Key Laboratory of Crystal Materials, Shandong University, 250100 Jinan, PR China
[d] College of Economy & Technology, Anhui Agricultural University, 230036 Hefei, PR China

ARTICLE INFO

*Article history:*
Received 14 July 2011
Accepted 30 October 2011
Available online 15 November 2011

*Keywords:*
Organotin(IV) carboxylates
Heterocyclic substituents
Crystal structure
Photoluminescence

ABSTRACT

Six novel organotin(IV) carboxylates have been successfully synthesized, namely, the polymer $(C_6H_5)_3Sn(L1)_\infty$ (**1**) [HL1 = 4-imidazolyl benzoic acid], the mononuclear $(C_6H_5)_3Sn(L2)$ (**2**) [HL2 = 4-pyrazolylbenzoic acid], $(C_6H_5)_3Sn(L3)\cdot CH_3OH$ (**3**) [HL3 = 4-triazolylbenzoic acid] and $(C_6H_5)_3Sn(L4)$ (**4**) [HL4 = 4-tetrazolyl benzoic acid] and the tetranuclear $[(n\text{-}Bu_2Sn)_4(L2)_2O_2(OCH_3)_2]$ (**5**) and $[(n\text{-}Bu_2Sn)_4(L3)_2O_2(OCH_3)_2]$ (**6**). X-ray diffraction analyses show 1D infinite chain of polymer **1**, single molecular structures of isomorphous complexes **2** and **4**, single molecule structures of complex **3** containing solvent $CH_3OH$ molecule and similar ladder-type structures of complexes **5** and **6**. The photoluminescence of ligands and **1–6** were also measured in the solid state at room temperature.



## 1. Introduction

The heterocyclic NO donor ligands play an important role in the development of coordination chemistry as they readily form complexes with most of metal ions [1–4]. The synthesis, structure and properties of coordination complexes still arouse considerable research interests because of their potential applications in material science [5]. Carboxylic acid is often used group for constructing new coordination compounds [6], in part because their various interactions to a single metal center or bridging interactions with multiple metal centers results in diverse topologies [7]. In addition, carboxylic acid can be used to assemble supramolecular structures through their ability to act as hydrogen bond acceptors and donors [8]. Likewise, pyrazole, imidazole, triazole and tetrazole heterocyclic ligands are small and simple, yet effective as bridging organic building blocks for coordination compounds [9]. A large number of one-, two- and three-dimensional infinite frameworks with azoles derivatives have been prepared and characterized because of the interest in their novel topologies [10].

Among main-group organometallic compounds, organotin has been receiving considerable attention in recent years [11], for some of them are biologically active or have been used as reagents or catalysts in organic reactions [12]. Furthermore, a surprisingly large structural diversity can be achieved by relatively simple synthetic variations from organotin compounds. Several novel cluster types such as ladder, drum, O-capped, cube, butterfly, triply- and doubly bridged ladders, have been assembled and structurally characterized [13]. Admittedly this field is quite nascent, but the recent results in this area are quite exciting.

In this contribution, six novel organotin(IV) carboxylates **1–6** were obtained by four carboxylic acids containing different azole groups and organotin [14]. The X-ray diffraction analysis reveal that both O donor atom and N donor atom take part in coordination with central metal Sn atom, which forms polymer **1** as a 1D infinite chain. While in the other five complexes, Sn only coordination with O donor atoms, which shows discrete structures with their own character. This work also provides useful information on the photoluminescence of these ligands and organotin complexes in the solid state.

## 2. Results and discussion

### 2.1. Crystal structure analysis

#### 2.1.1. Polymer *1*

The X-ray single crystal reveals that polymer **1** is a successive and uninterrupted entity. It crystallizes in the monoclinic with space group *P*2(1)/*c*. The unit consists of one Sn atom connecting three C from different phenyl rings, one O(1) atom from HL1 and one N(1) atom from next HL1 as shown in Fig. 1(a). HL1 in polymer **1** indicates a severe distortion with the dihedral angles between imidazole ring and the central phenyl unit to be 53.35°, while this

* Corresponding authors. Tel.: +86 5515108151; fax: +86 5515107342.
*E-mail addresses:* zhpzhp@263.net (H.-P. Zhou), yptian@ahu.edu.cn (Y.-P. Tian).

0277-5387/$ - see front matter © 2011 Published by Elsevier Ltd.
doi:10.1016/j.poly.2011.10.032

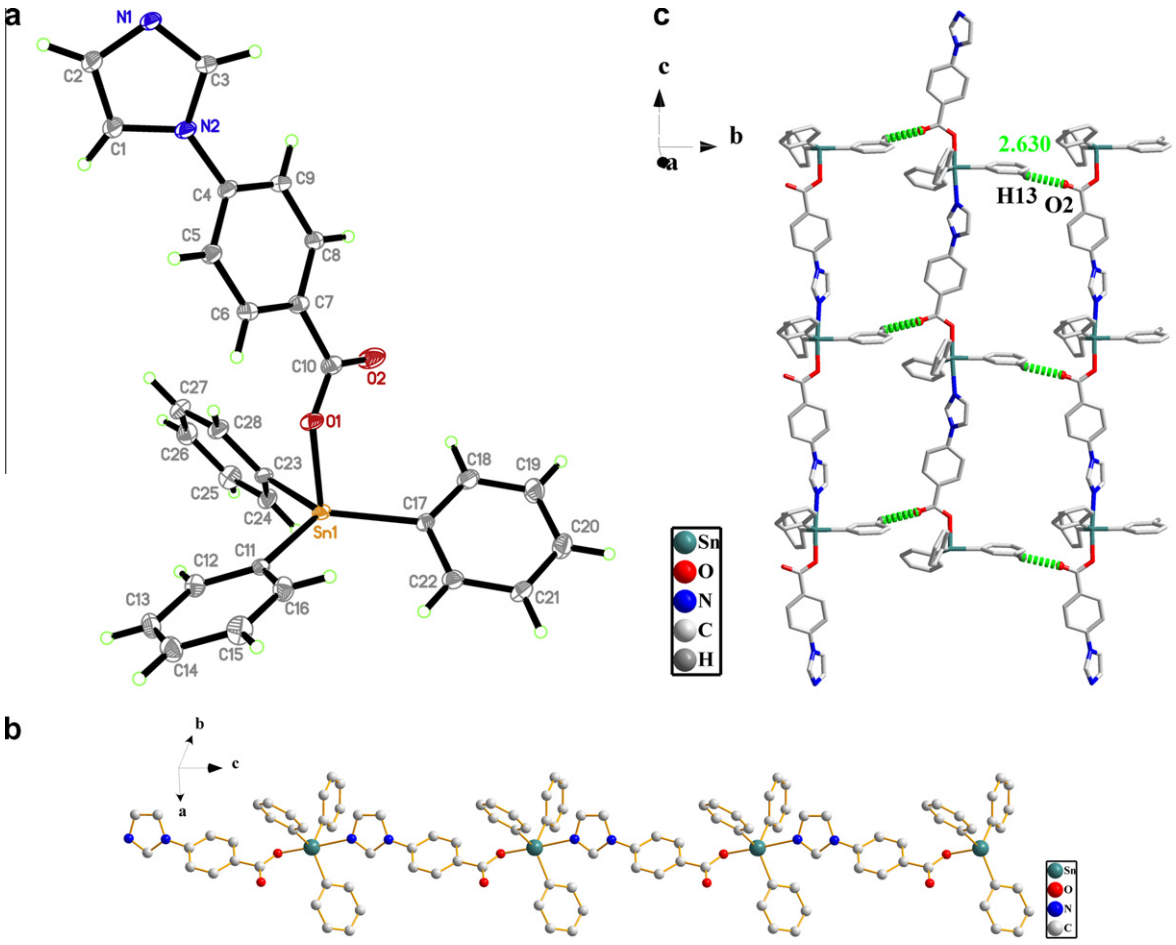


**Fig. 1.** (a) ORTEP diagram showing the structures of polymer **1**. (b) The 1D linear chain of polymer **1** along the *c*-axis. (c) The 2D network of polymer **1** showing the weak C–H···O interactions along the *b*-axis, respectively. Only H atoms that were from hydrogen bonds were saved.

is 13.67° in the free ligand [15]. Thus it can be seen that HL1 was change its planarity due to meeting the coordination requirements of steric hindrance. The influence of the Sn(1)–N(1) coordination bond causes the concomitant contraction in the tetrahedral angles around the central Sn(1) of polymer **1** (the angles are 90.23°, 94.04°, and 97.54°, respectively). O(2) atom approaches the Sn(1) atom at a distance of 3.310 Å, which is less than the sum of their van der Waals radii for Sn and O atoms (3.680 Å) [16]. The coordination environment of polymer **1** has quite distorted trigonal bipyramidal geometry. Polymer **1** form a 1D infinite chain by the metal-bound peripheral imidazole-N(1) and carboxyl-O(1) running along the *c*-axis (Sn(1)–N(1) = 2.620 Å, Sn(1)–O(1) = 2.164 Å) as shown in Fig. 1(b). And then, 2D network is generated by lots of 1D linear chains, which connect to each other via hydrogen bonds along the *b*-axis as seen from Fig. 1(c). The hydrogen bond is between the non-coordinating O(2) atom and the phenyl substituent on the tin atom in an adjacent chain [$d$(C(13)···O(2)) = 3.354 Å, $d$(H(13)···O(2)) = 2.630 Å, ∠(C(13)–H (13)···O(2)) = 135.16°]. It is observed from the *ab*-plane that the three phenyls substituent on the tin atom in each neighboring chain are arranged as "clover", positive and inverted positions are alternate along the *a*-axis. There is some evidence of a weak C–H···π interaction between C(2)–H(2) of imidazole ring and the phenyl of ligand in an adjacent chain to be 3.130 Å. Besides, an additional weak C–H···π interactions between phenyls substituent on the tin and imidazole ring is 3.209 Å along the *b*-axis. The molecules of adjacent layers are stacked as sandwich. Both the weak C–H···π interactions contribute to stabilizing 3D architecture along the *a*-axis and *b*-axis.

### 2.1.2. Complex **2**

Complex **2** crystallizes in the monoclinic with space group *P*2(1)/*c* and shows a discrete structure in accordance with the preference of such structures for triphenyltin arylcarboxylates. HL2 in complex **2** indicates a smaller distortion with the dihedral angles between pyrazole ring and the central phenyl unit to be 15.42°. As shown in Fig. 2(a), there is four coordinated bonds around central Sn atom, namely, three Sn–$C_{ph}$ bonds and one Sn–$O_{carboxyl}$ bond. The bond lengths of Sn(1)–C(11), Sn(1)–C(17) and Sn(1)–C(23) are 2.134, 2.114 and 2.138 Å, respectively, which are not sensitive to changes of coordination. Moreover, the tetrahedral angles around the central Sn (97.76°, 108.12° and 110.70°) are all in normal range [17]. Two types of Sn–O bond lengths are found: Sn(1)–O(1) 2.058 Å and Sn(1)–O(2) 2.725 Å. Actually, 2.725 Å is considered long for primary Sn–O bonding, but represents a type of secondary interaction [18].

Complex **2** can be referred to an idealized geometry in which the Sn is involved in four covalent bonds having a distorted tetrahedral geometry about the tin center, while the carboxyl oxygen atom is involved in a fifth weaker bonding interaction with tin in which it approaches a tetrahedral face. The pyrazolylbenzoic system and the Sn–$C_{ph}$ bond opposite the aforementioned tetrahedral face tend toward coplanarity. Therefor, in this structural representation, complex **2** was described as distorted trigonal-bipyramidal geometry with five-coordinated tin center (Scheme 1) [19].

Weak interactions play significant roles in forming the topological structures. Adjacent molecules are interacted with each other through hydrogen bonds forming a 1D chain structure along the *a*-axis (Fig. 2(b)). The oxygen atom of the ligand is the H bonding

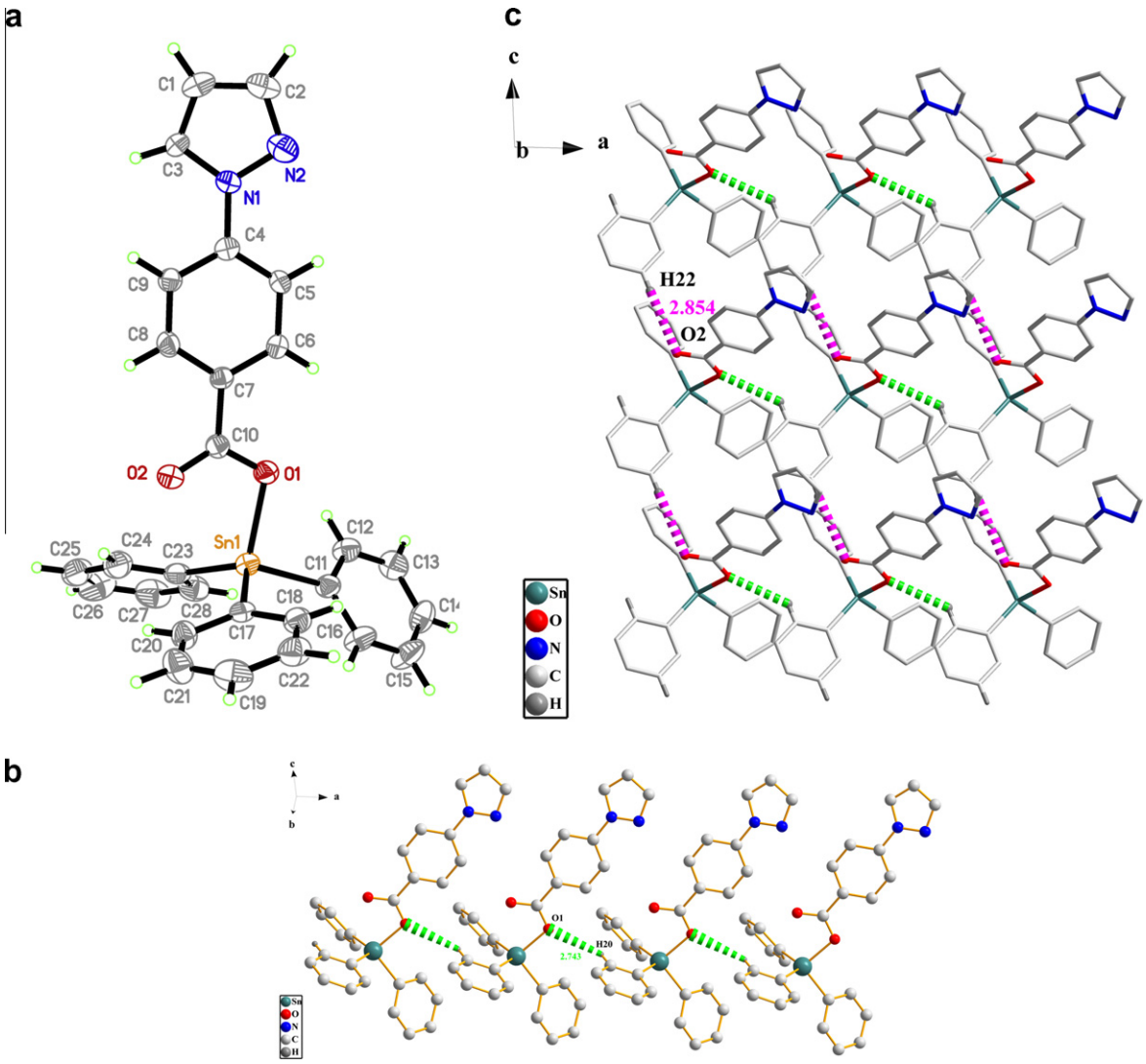


**Fig. 2.** (a) ORTEP diagram showing the structures of complex **2**. (b) The 1D chain of complex **2** showing C–H···O interactions along the *a*-axis. (c) The 2D (4,4)-network of complex **2** showing the weak C–H···O interactions along the *c*-axis. Only H atoms that were from hydrogen bonds were saved.

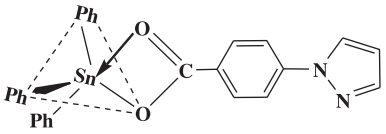


**Scheme 1.** Schematic representation of distortion in complex **2**.

acceptor, and the H(C) donor is from the phenyl substituent on the tin atom [$d$(C(20)···O(1)) = 3.434 Å, $d$(H(20)···O(1)) = 2.743 Å, ∠(C(20)–H (20)···O(1)) = 131.82°] [20]. As shown in Fig. 2(c), the 1D chains further link along the *c*-axis direction to form a 2D net-like structure through rather weak C–H···O interactions with the H from the phenyl substituent on the Sn and the O from carboxyl [$d$(C(22)···O(2)) = 3.743 Å, $d$(H(22)···O(2)) = 2.854 Å, ∠(C(22)–H(22)···O(2)) = 160.01°]. Finally, the extended 3D topological structures were formed via π···π stacking interactions between the phenyl of the ligand and the pyrazole ring in neighboring chains with distance of 3.701 Å and an angle of 15.45° [21]. The π···π stacking interactions between layer and layer are the most important interactions, which contribute greatly to the supramolecular topologies. While the rather weak C–H···O interaction has a C(22)···O(2) distance of 3.743 Å, which is shorter than the most forgiving contact distance of <4 Å, but beyond the widely accepted range of distances between 3.1 and 3.5 Å [22]. So this rather weak C–H···O interaction may be simply consequences of other packing interactions.

### 2.1.3. Complex **3**

The X-ray structure of the resultant metal-complex reveals triclinic mononuclear structure with space group $P\bar{1}$. Though complex **3** has a discrete structure, the coordination mode is different from that of complex **2**. The coordination mode of complex **3** has three phenyl bonded on the Sn(IV), one ligand (HL3) and one methanol as oxygen donors to the metal center, respectively. HL3 in complex **3** possesses perfect planarity with the dihedral angles between triazole ring and the central phenyl unit to be 8.80°. Moreover, tetrahedral angle around the Sn atom is in the range of 91.42–100.93°. The distance of Sn(1)–O(1) bond is 2.098 Å, while O(2) atom approaches the Sn(1) atom at a distance of 3.023 Å, which is longer than that of complex **2** (2.725 Å). The secondary interaction of Sn(1)···O(2) in complex **3** may be impair by five-coordination bonds around tin center. Solvent $CH_3OH$ molecule coordinates to the Sn atom with the bond length of 2.532 Å and adopts opposite direction of HL3.

Complex **3** indicates a little distorted trigonal bipyramidal geometry as shown in Fig. 3(a). A 1D chain is formed through C–H···O interactions along the *a*-axis just like that in complex **2**, as shown in Fig. 3(b). The O(2)···H(24) contact is 2.590 Å, and C(24)–H(24)···O(2) angle is 161.72°. Adjacent chains linked through O–H···N hydrogen bonds (H(100)···N(3) = 1.829 Å and the angle to be 171.67°) generate a 2D framework along the *c*-axis (Fig. 3(c)). Solvent $CH_3OH$ molecule plays an important role in forming the 2D framework [23]. Moreover, the stacking manner was given by evidence of C–H···π stacking interactions (3.141 Å) among phenyl units to lead to the 3D architecture. In addition, C–H···O interactions (H(5)···O(5) = 2.650 Å and the angle to be 117.62°) also contribute greatly to the supramolecular topologies.

### 2.1.4. Complex *4*

Complex **4** is isomorphous with complex **2**. It crystallizes in the monoclinic space group *P*2(1)/*c* with one molecule in the asymmetric unit. To a first approximation, there are four coordinated bonds around the Sn atom, namely, three ipso-C atoms of the phenyl groups and the O atom (Sn(1)–O(2) 2.068 Å) of HL4 as shown in Fig. 4(a). The dihedral angles between tetrazole ring and phenyl of ligand is 2.24°, which shows a good planarity after coordination [24]. Two types of Sn–O bond lengths are found: Sn(1)–O(2) 2.068 Å and Sn(1)–O(1) 2.749 Å. Although not considered to represent a significant bonding interaction, the influence of the O(1) atom is such that it causes the expansion of the O(2)–Sn(1)–C(14) angle 109.10° and the concomitant contraction in the C(20)–Sn(1)–O(2) angle 97.66°. Support for the conclusion that the O(2) atom does not form a coordinated bond with tin is found in the disparity in the C(7)–O(1) and C(7)–O(2) bond distance of 1.219 and 1.315 Å, respectively [25]. However, the significant interactions of Sn(1)–O(1) cannot be neglected and complex **4** was described as distorted trigonal-bipyramidal geometry. As shown in Fig. 4(b), the 1D chains along the crystallographic *a*-axis connected through C–H···O (H(13)···O(2) is 2.760 Å and the C(13)–H(13)···O(2) angle is 131.84°) resemble that of complex **2**. But in a further investigation, the weak interactions which construct supramolecular structure are different from complex **2**. A pair of C–H···π interactions (2.948 Å) exist in the two molecules which locate a position as "head to head". And there are another C–H···π interactions (2.698 Å) which connect two parallel compounds of adjacent chains. Consequently, it forms a building block with the ligand unit in the middle and the phenyls substituent on the tin in both sides. Then the adjacent building block connect to each other with weak C–H···π interactions (3.495 Å) in *bc*-plane (Fig. 4(c)). Weak C–H···π interaction plays a vital role in determining the crystal packing and in the construction of the extended 3D supramolecular network.

### 2.1.5. Complex *5*

Complex **5** crystallizes in the triclinic with space group $P\bar{1}$. The centrosymmetric structure features a central $Bu_4Sn_2O_2$ core to which two $Bu_2Sn$ entities are linked with the result that the O(5) and O(5A) atoms are three coordinate [26]. Each of the independent tin atoms in the structure exhibits distorted trigonal bipyramidal geometry, with a $C_2O$ trigonal plane and axial positions that are occupied by oxygen atoms. The formation of the dimeric

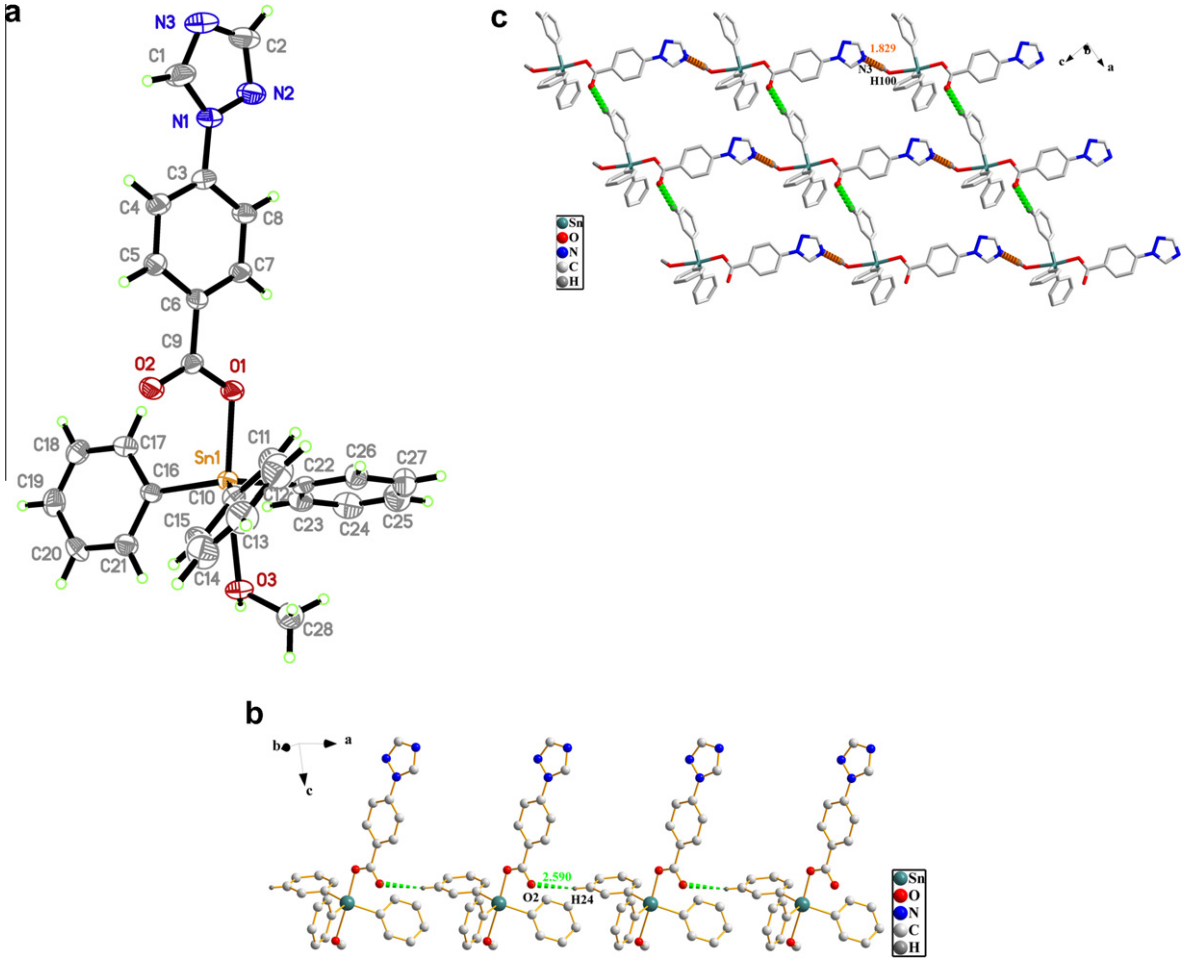


**Fig. 3.** (a) ORTEP diagram showing the structures of complex **3**. (b) The 1D chain of complex **3** showing C–H···O interactions along the *a*-axis. (c) The 2D network of complex **3** showing the weak O–H···N interactions along the *c*-axis. Only H atoms that were from hydrogen bonds were saved.

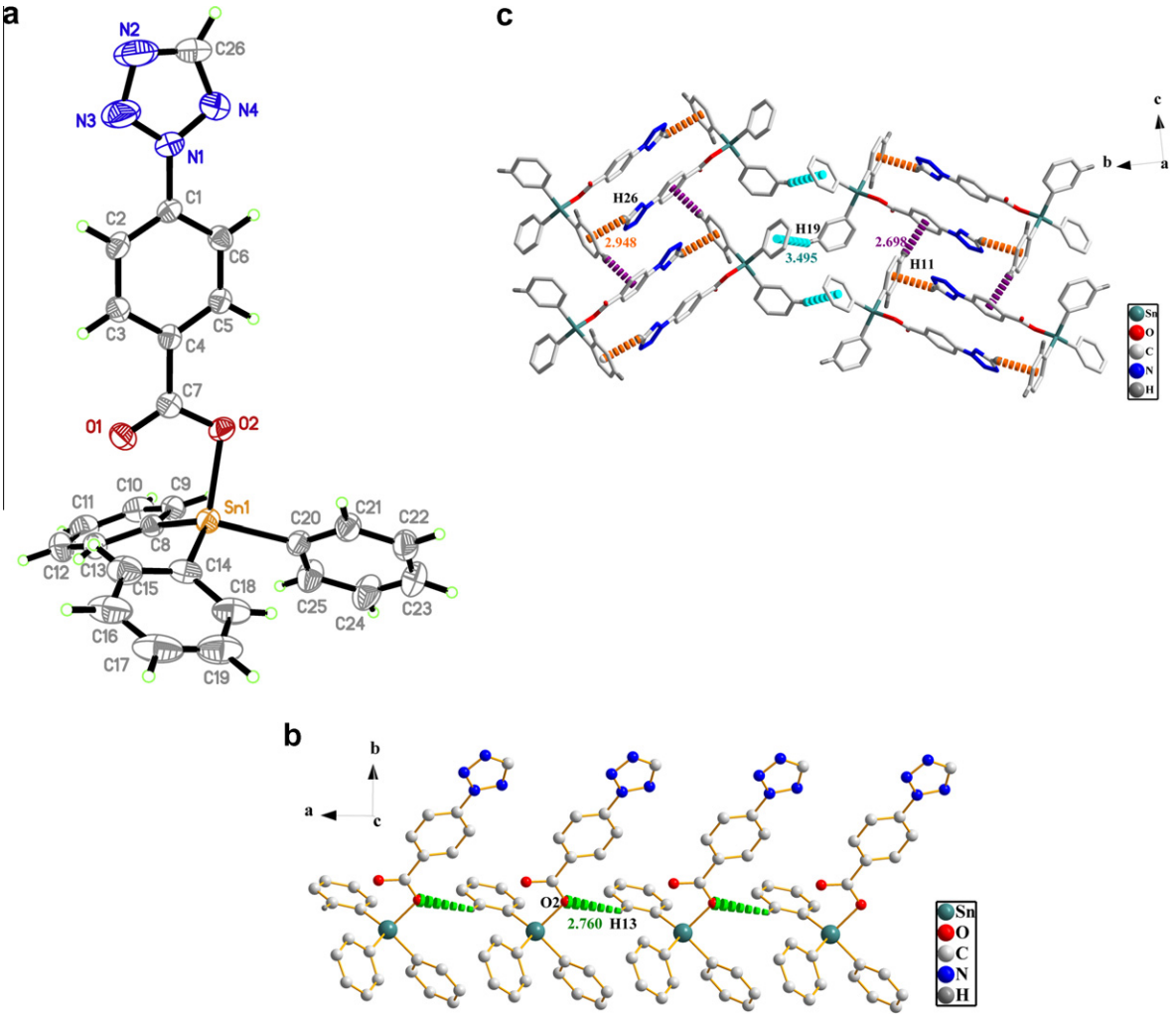


**Fig. 4.** (a) ORTEP diagram showing the structures of complex **4**. (b) The 1D chain of complex **4** showing C–H···O interactions along the *a*-axis. (c) The 2D network of complex **4** showing the weak C–H···π interactions along the *c*-axis and the weak C–H···π interactions along the *b*-axis. Only H atoms that were from hydrogen bonds were saved.

distannoxanes **5** represents an example of ladder-type carboxylates in which the insertion of $\mu_2$-$OCH_3$ group occurs. This result can be interpreted in terms of donor strength competition, in which the –$OCH_3$ groups show higher donor capacity than the carboxylato group of the ligand [27]. It is noteworthy that the complex **5** crystal unit of the former containing two molecules and the two molecules are approximately perpendicular distribution to each other as shown in Fig. 5(a). Through three types of C–H···O hydrogen bonding (C(50)–H(50A)···O(3) = 3.505 Å, H(50A)···O(3) = 2.564 Å, angle to be 163.68°; C(15)–H(12)···O(2) = 3.235 Å, H(15)···O(2) = 2.310 Å, angle to be 172.34°; C(12)–H(12)···O(2) = 3.440 Å, H(12) ···O(2) = 2.538 Å, angle to be 163.19°), the adjacent molecules formed into a 1D structure along the *a*-axis as seen from Fig. 5(b). Also contributed by C–H···π weak interactions between pyrazole ring and the primary C(H) of *n*-Bu in neighboring chains with the distance of 2.733 Å, a 2D network structure is produced along *b*-axis Fig. 5(c). And then, the 3D architecture was formed by evident of C–H···π weak interactions (3.199 Å) between C(H) of pyrazole ring and the phenyl of ligand.

### 2.1.6. Complex **6**

Compared with complex **5**, complex **6** is also in the triclinic space group $P\bar{1}$ and has the same coordination mode. The substitution of pyrazole for triazole brought about a little change of the molecular stacking. The complex **6** crystal unit of the former contain only one molecule, which is simpler than that of complex **5** (Fig. 6(a)). The crystal structure of **6** also shows a ladder framework and features a $\mu_2$-coordination of –$OCH_3$. Each methanol molecule adopts anisobidentate chelating coordination modes (Sn(4)–O(7) 2.220 Å and Sn(3)–O(7) 2.132 Å), while the carboxylic groups of 4-triazolebenzoic acid ligand coordinate with Sn atom as a unidentate bonding (Sn(4)–O(3) 2.153 Å); these values fall in the typical Sn–O bond length range. Seen along the *b*-axis in Fig. 6(b), the molecules of complex **6** connect each other through C–H···O weak interactions with distance of 3.324 Å (the distance of H(2)···O(4) to be 2.400 Å, angle to be 172.32°), which leads to a 1D chain structure. Furthermore, C–H···N weak interactions between adjacent 1D chains are involved in both C(4)–H(4)···N(2) with the distance of 3.598 Å (the distance of H(4)···N(2) to be 2.712 Å, angle to be 159.39°) along *b*-axis as well as C(26)–H(26A)···N(3) with the distance of 3.412 Å (the distance of H(26A)···N(3) to be 2.561 Å, angle to be 147.94°) along *c*-axis, which generates a 2D network structure (Fig. 6(c)). An additional further C–H···π interactions between the phenyl of the ligand and the primary C(H) of *n*-Bu in neighboring chains lead to a 3D layer frameworks; the C–H···π distance is 3.065 Å.

Details of the relevant data collection and refinement are summarized in Table 1. Selected bond lengths and bond angles for **1**–**6** are listed in Table 2.

Making a comparison among compounds **1**–**4**, polymer **1** is the special one. Notably, not only O atom but also N atom takes part in coordination with central metal Sn atom, which forms a successive

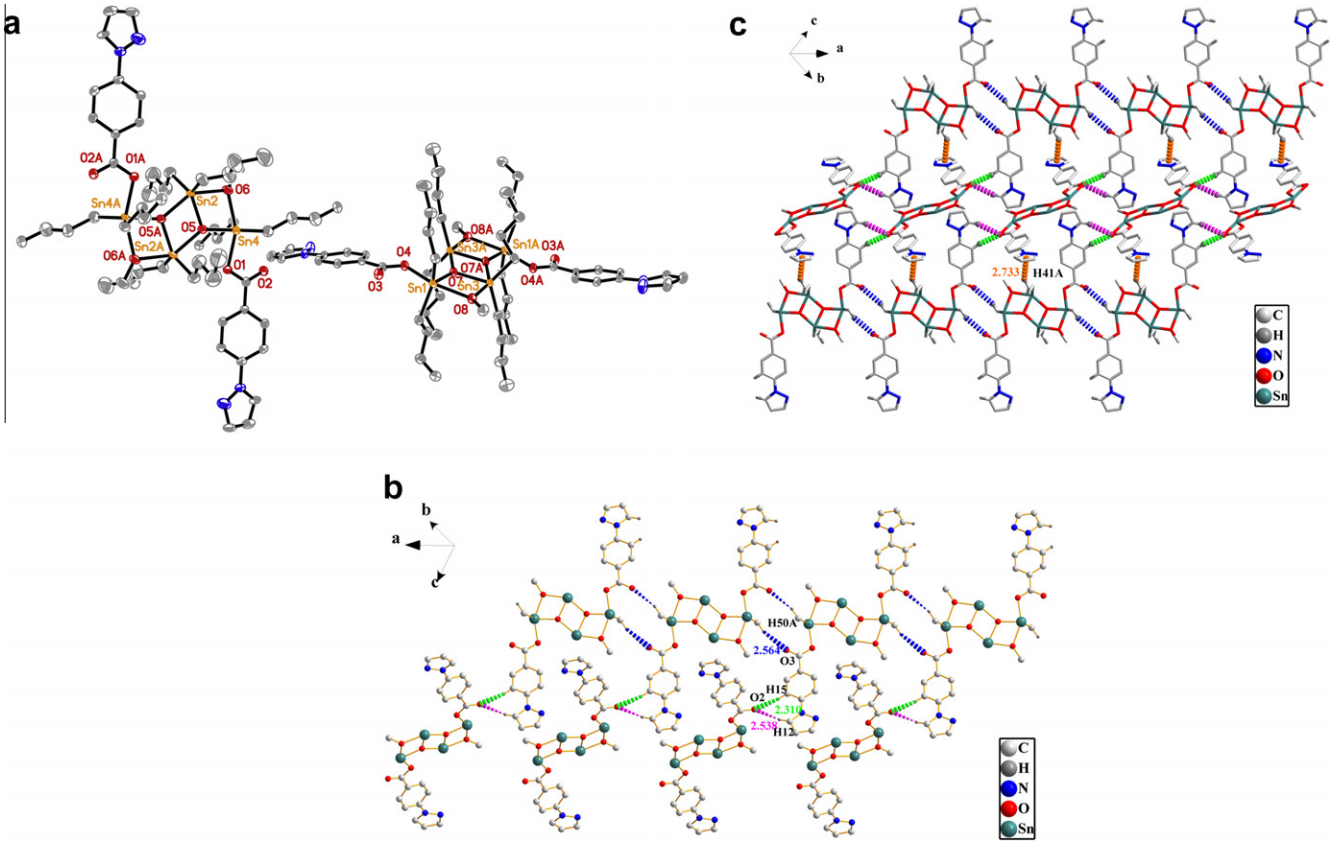


**Fig. 5.** (a) ORTEP diagram showing the structures of complex **5**. (b) The 1D ladder of complex **5** showing C–H···O interactions along the *a*-axis. (c) The 2D network of complex **5** showing the weak C–H···π interactions along the *b*-axis. Only H atoms that were from hydrogen bonds were saved.

and uninterrupted line-type polymer. The formation of this unusual geometry may be due to the reasons as below: the two nitrogen atoms in pyrazole are ortho position and meta position in imidazole, namely, $\mu_1$ and $\mu_3$. So the steric hindrance of the latter one is smaller than the former and it allows the nitrogen on $\mu_3$ to be a coordination site to bind metals. The added nitrogen atoms rather than that $\mu_3$ in triazole and tetrazole increase the capability for attracting electrons, which adversely affects the ability to coordinate with metals [28]. Therefore, in our reported compounds, only HL1 containing imidzole can coordinate with Sn to form linear coordination polymer.

In some extent, ligands consisting of both imidazole and carboxylate as building block may have a tendency to form polymer. While the central metal Sn atom only coordinates with O donor atoms of other three complexes, which display diversiform discrete structures with their own character. The crystal structure of complex **2** and **4** are similar to each other. We can conclude that complexes **2** and **4** are five-coordinated because of values of $\delta$ ($^{119}$Sn) of **2** and **4** are −107.8 and −101.7 ppm, respectively [29,30]. The Sn atom has four covalent bonds and a fifth weaker bonding interaction, which form distorted trigonal bipyramidal geometry. Solvent molecule plays an important role in constructing the 3D framework in complex **3**. Taking complexes **5** and **6** into account, we use the same *n*-$Bu_2SnO$ and make the nitrogen heterocyclic ring group of the ligands be different. Although the coordination modes are the same, the supramolecular structures vary. The structure of **5** is more complicated than that of **6**, for the simple reason that the crystal unit of the former one containing two molecules yet the latter one containing only one molecule.

From above, we can safely propose that the selection of the nitrogen heterocyclic ring can definitely adjust the topologies of coordination frameworks. Just subtle variations of nitrogen heterocyclic ring not only affect the coordinated bonds of entities, but also affect various individual interactions, such as C–H···O, C–H···N, O–H···N, C–H···π and π···π stacking interactions, which influence the final supramolecular assembly.

### 2.2. Optical properties

There is considerable contemporary interest in the development of new organic/organometallic luminescent compounds. This is because of the enormous potential of such materials in niche technological applications based on the possibility of using them as photo- and electroluminescent devices [31]. Therefore the photoluminescence properties of the ligands and complexes were measured in the solid state at room temperature. The nanosecond range of lifetime in the solid state at 298 K reveals that the emission is fluorescent in nature. The measurements were carried out under the same experimental conditions.

In comparison with HL1 with an emission maximum at 481 nm, polymer **1** exhibits strongly blue shift with emissions at 369 nm, upon excitation at 320 nm. As shown above, the L1 in polymer **1** is more twisted and resulted in a larger energy gap between $\pi^*$ and $\pi$ orbitals, which could give rise to the emission wavelength of polymer **1** blue-shifted [32].

Complexes **2** and **5** exhibit photoluminescence with emissions at 347 and 340 nm, respectively, upon excitation at 320 nm, which indicate blue shift comparing with that of HL2 with an emission maximum at 361 nm under the same excitation wavelength. The emission maximum of complexes **6** is at 366 nm, which has no shift basically comparing with that of HL3 (368 nm). For complexes **4**, blue emissions with maxima at 483 nm were observed upon

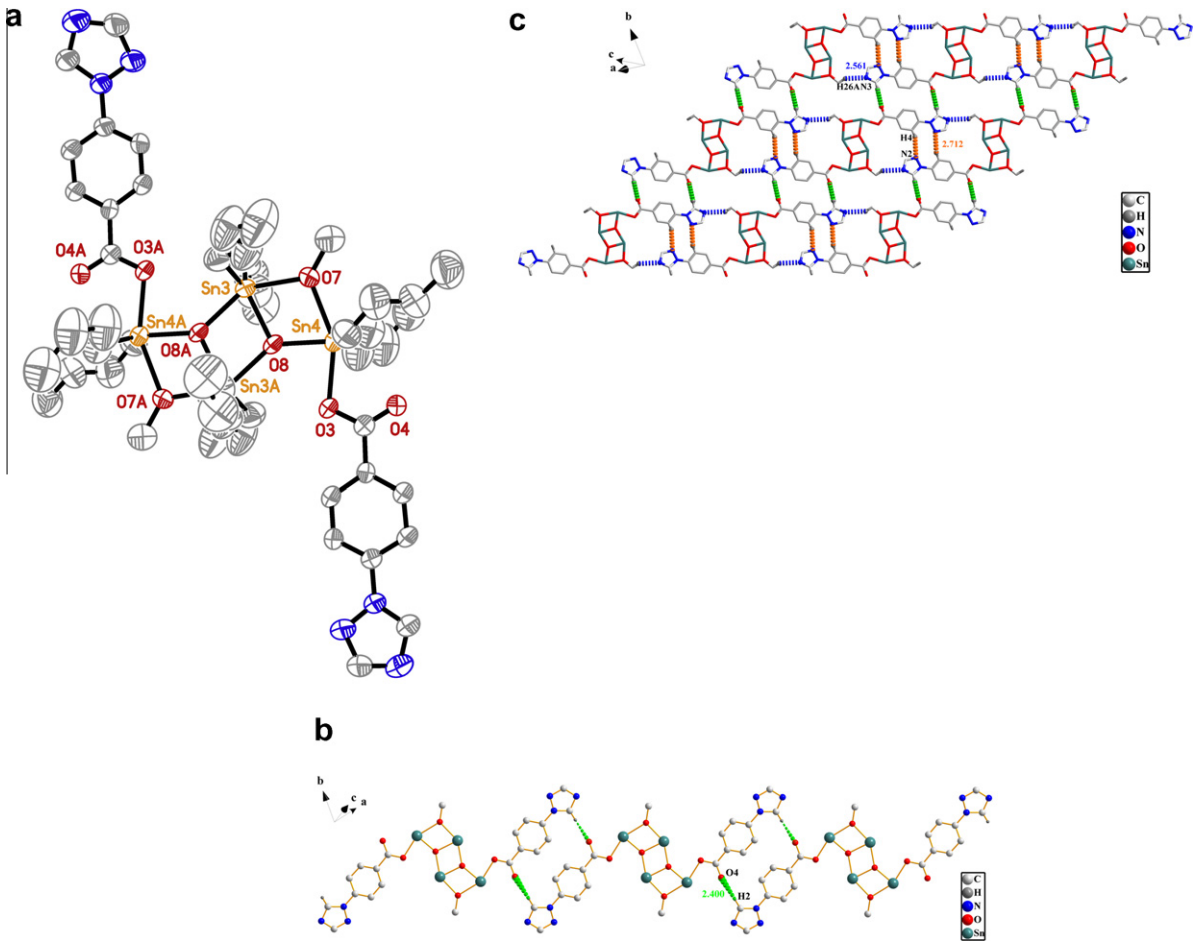


**Fig. 6.** (a) ORTEP diagram showing the structures of complex **6**. (b) The 1D ladder of complex **6** showing C–H···O interactions along the *b*-axis. (c) The 2D network of complex **6** showing the weak C–H···N interactions along the *b*-axis and *c*-axis. Only H atoms that were from hydrogen bonds were saved.

**Table 1**
Crystal data and details of structure refinement parameters for complexes **1**–**6**.

| Compound | **1** | **2** | **3** | **4** | **5** | **6** |
|---|---|---|---|---|---|---|
| Formula | $C_{28}H_{22}N_2O_2Sn$ | $C_{28}H_{22}N_2O_2Sn$ | $C_{28}H_{25}N_3O_3Sn$ | $C_{26}H_{20}N_4O_2Sn$ | $C_{54}H_{92}N_4O_8Sn_4$ | $C_{52}H_{90}N_6O_8Sn_4$ |
| Formula weight | 537.17 | 537.17 | 570.20 | 539.15 | 1400.08 | 1402.06 |
| Crystal system | monoclinic | monoclinic | triclinic | monoclinic | triclinic | triclinic |
| Space group | $P2(1)/c$ | $P2(1)/c$ | $P\bar{1}$ | $P2(1)/c$ | $P\bar{1}$ | $P\bar{1}$ |
| $a$ (Å) | 9.816(5) | 6.779(5) | 10.108(5) | 6.792(5) | 11.946(5) | 11.821(5) |
| $b$ (Å) | 18.729(5) | 42.144(5) | 10.282(5) | 41.628(5) | 14.429(5) | 12.219(5) |
| $c$ (Å) | 14.288(4) | 8.549(5) | 12.446(5) | 8.577(5) | 21.175(5) | 12.345(5) |
| $\alpha$ (°) | 90.000(5) | 90.000(5) | 85.768(5) | 90.000(5) | 74.530(5) | 63.800(5) |
| $\beta$ (°) | 118.080(2) | 93.839(5) | 83.055(5) | 94.557(5) | 75.566(5) | 89.167(5) |
| $\gamma$ (°) | 90.000(5) | 90.000(5) | 86.425(5) | 90.000(5) | 66.114(5) | 85.404(5) |
| $V$ (Å$^3$) | 2317.6(16) | 2437(2) | 1278.7(10) | 2417(2) | 3174.8(19) | 1594.3(11) |
| $Z$ | 4 | 4 | 2 | 4 | 2 | 1 |
| $D_{calc}$ (mg m$^{-3}$) | 1.539 | 1.464 | 1.481 | 1.481 | 1.465 | 1.460 |
| $\mu$ (mm$^{-1}$) | 1.130 | 1.075 | 1.033 | 1.086 | 1.604 | 1.598 |
| $\theta$ range (°) | 1.95–25.00 | 0.97–25.00 | 1.99–25.00 | 0.98–24.99 | 1.97–25.00 | 1.73–25.00 |
| Total No. of data | 15636 | 28223 | 8884 | 16925 | 22528 | 11136 |
| No. of unique data | 4083 | 4289 | 4418 | 4252 | 11062 | 5538 |
| No. of parameters refined | 298 | 298 | 320 | 299 | 661 | 321 |
| $R_1$ | 0.0258 | 0.0409 | 0.0483 | 0.0400 | 0.0354 | 0.0596 |
| $wR_2$ | 0.0515 | 0.1220 | 0.1217 | 0.1197 | 0.0870 | 0.1597 |
| Goodness-of-fit (GOF)on $F^2$ | 1.028 | 0.961 | 1.047 | 0.947 | 0.992 | 0.959 |

excitation at 395 nm, while free ligand HL4 displays two emissions at 444 nm and 468 m under the same conditions. The observed emissions above are probably contributed by the π–π* intraligand fluorescence since similar emissions were also observed for corresponding ligands themselves [33].

$\lambda_{em}$ of complexes **3** was located at 421 nm while that of HL3 was at 368 nm, which can be tentatively assigned to a MLCT based on a significant red shift from HL3 to **3** [34].

The emission range varied extensively, which was considered to mainly originate from the influence of the coordination modes of

**Table 2**
Metric parameters for the molecular structures of **1**–**6**.

| Compound | Coordination mode of the carboxylate ligand and coordination environment around tin | Sn–O (carboxylate) bond lengths (Å) | Lengths of covalent bond around tin (Å) | Bond angles (°) |
|---|---|---|---|---|
| **1** | Monodentate pentacoordinate (3C, O, N) distorted trigonal-bipyramidal | Sn(1)–O(1) 2.164(2)<br>Sn(1)···O(2) 3.311(5) | Sn(1)–O(1) 2.164(2)<br>Sn(1)–N(1)$^{\#1}$ 2.475(2)<br>Sn(1)–C(11) 2.137(3)<br>Sn(1)–C(17) 2.128(3)<br>Sn(1)–C(23) 2.141(3) | C(11)–Sn(1)–O(1) 90.2(1)<br>C(17)–Sn(1)–O(1) 97.5(6)<br>C(23)–Sn(1)–O(1) 93.9(5) |
| **2** | Anisobidentate chelating pentacoordinate (3C, 2O) distorted trigonal-bipyramidal | Sn(1)–O(1) 2.058(3)<br>Sn(1)–O(2) 2.725(5) | Sn(1)–O(1) 2.058(3)<br>Sn(1)–C(11) 2.134(5)<br>Sn(1)–C(17) 2.114(5)<br>Sn(1)–C(23) 2.138(5) | O(1)–Sn(1)–C(17) 108.1(2)<br>O(1)–Sn(1)–C(11) 97.7(6)<br>O(1)–Sn(1)–C(23) 110.6(9) |
| **3** | Monodentate pentacoordinate (3C, O, O) distorted trigonal-bipyramidal | Sn(1)–O(1) 2.098(3)<br>Sn(1)···O(2) 3.023(5) | Sn(1)–O(1) 2.098(3)<br>Sn(1)–O(3) 2.533(4)<br>Sn(1)–C(10) 2.122(5)<br>Sn(1)–C(16) 2.128(5)<br>Sn(1)–C(22) 2.126(5) | O(1)–Sn(1)–C(10) 98.1(8)<br>O(1)–Sn(1)–C(16) 100.9(4)<br>O(1)–Sn(1)–C(22) 91.4(2) |
| **4** | Anisobidentate chelating pentacoordinate (3C, 2O) distorted trigonal-bipyramidal | Sn(1)–O(2) 2.068(3)<br>Sn(1)–O(1) 2.749(3) | Sn(1)–O(2) 2.068(3)<br>Sn(1)––C(8) 2.120(5)<br>Sn(1)–C(14) 2.138(5)<br>Sn(1)–C(20) 2.135(5) | O(2)–Sn(1)–C(8) 108.4(8)<br>O(2)–Sn(1)–C(14) 109.1(0)<br>O(2)–Sn(1)–C(20) 97.6(6) |
| **5** | Monodentate pentacoordinate (2C, O, 2O) distorted trigonal-bipyramidal | A<br>Sn(1)–O(4) 2.154(3)<br>Sn(1)···O(3) 2.974(5) | A<br>Sn(1)–O(4) 2.154(3)<br>Sn(1)–O(7) 2.022(3)<br>Sn(1)–O(8) 2.240(3)<br>Sn(1)–C(36) 2.130(5)<br>Sn(1)–C(50) 2.128(5) | A<br>O(7)–Sn(1)–O(4) 80.7(6)<br>C(50)–Sn(1)–O(4) 96.6(5)<br>C(36)–Sn(1)–O(4) 100.9(8)<br>O(4)–Sn(1)–O(8) 151.8(6)<br>O(7)–Sn(1)–O(8) 71.5(3)<br>C(50)–Sn(1)–O(8) 90.1(3)<br>C(36)–Sn(1)–O(8) 94.4(5)<br>O(7)–Sn(1)–C(50) 113.6(0)<br>O(7)–Sn(1)–C(36) 113.1(6)<br>C(50)–Sn(1)–C(36) 131.9(6) |
| | | B<br>Sn(4)–O(1) 2.153(3)<br>Sn(4)···O(2) 2.874(5) | B<br>Sn(4)–O(1) 2.153(3)<br>Sn(4)–O(5) 2.012(3)<br>Sn(4)–O(6) 2.237(3)<br>Sn(4)–C(21) 2.119(6)<br>Sn(4)–C(25) 2.130(5) | B<br>O(5)–Sn(4)–C(21) 113.2(2)<br>O(5)–Sn(4)–C(25) 114.5(0)<br>C(21)–Sn(4)–C(25) 130.8(2)<br>O(5)–Sn(4)–O(1) 81.1(5)<br>C(21)–Sn(4)–O(1) 98.2(4)<br>C(25)–Sn(4)–O(1) 100.1(4)<br>O(5)–Sn(4)–O(6) 71.6(3)<br>C(21)–Sn(4)–O(6) 91.9(2)<br>C(25)–Sn(4)–O(6) 91.9(8)<br>O(1)–Sn(4)–O(6) 152.7(7) |
| **6** | Monodentate pentacoordinate (2C, O, 2O) distorted trigonal-bipyramidal | Sn(4)–O(3) 2.153(6)<br>Sn(4)···O(4) 2.879(5) | Sn(4)–O(3) 2.153(6)<br>Sn(4)–O(7) 2.221(7)<br>Sn(4)–O(8) 2.010(6)<br>Sn(4)–C(13) 2.125(2)<br>Sn(4)–C(14) 2.029(2) | O(8)–Sn(4)–O(3) 82.5(2)<br>C(14)–Sn(4)–O(3) 102.6(6)<br>O(3)–Sn(4)–O(7) 153.7(2)<br>C(13)–Sn(4)–O(3) 96.5(5)<br>C(13)–Sn(4)–O(7) 93.0(5)<br>C(14)–Sn(4)–O(7) 89.3(6)<br>O(8)–Sn(4)–O(7) 71.2(3)<br>C(14)–Sn(4)–C(13) 130.9(7)<br>O(8)–Sn(4)–C(14) 116.0(6)<br>O(8)–Sn(4)–C(13) 111.1(5) |

Symmetry transformations used to generate equivalent atoms: #1 $x+1, y, z+1$.

metal atom and diverse intermolecular interactions in the solid state [35].

## 3. Conclusions

Complexes **1**–**6** are synthesized based on the functional ligands (HL1–HL4) and $Ph_3Sn(OH)$ or $n$-$Bu_2SnO$. X-ray diffraction analyses show the novel structures of compounds **1**–**6** with 1D infinite chain of polymer **1**, single molecular structures of complex **2** and **4**, containing solvent molecule of complex **3** and similar structures of complex **5** and **6**. In some extent, ligands consisting of both imidazole and carboxylate as building block may have a tendency to form polymer. Just subtle variations of nitrogen heterocyclic ring not only affect the coordinated bonds of entities, but also affect various individual interactions, such as C–H···O, C–H···N, O–H···N, C–H···π and π···π stacking interactions, which influence the final supramolecular assembly. At the same time, solvent molecule plays an important role in forming the 3D framework. In addition, this article provides useful information on the photoluminescence. The emission range varied extensively, which was considered to mainly originate from the influence of the coordination modes of metal atom and diverse intermolecular interactions in the solid state.

## 4. Experimental

### 4.1. Materials and methods

The reagents and solvents employed were commercially available and used as received without further purification. The synthetic route complexes are presented in Scheme 2. IR spectra

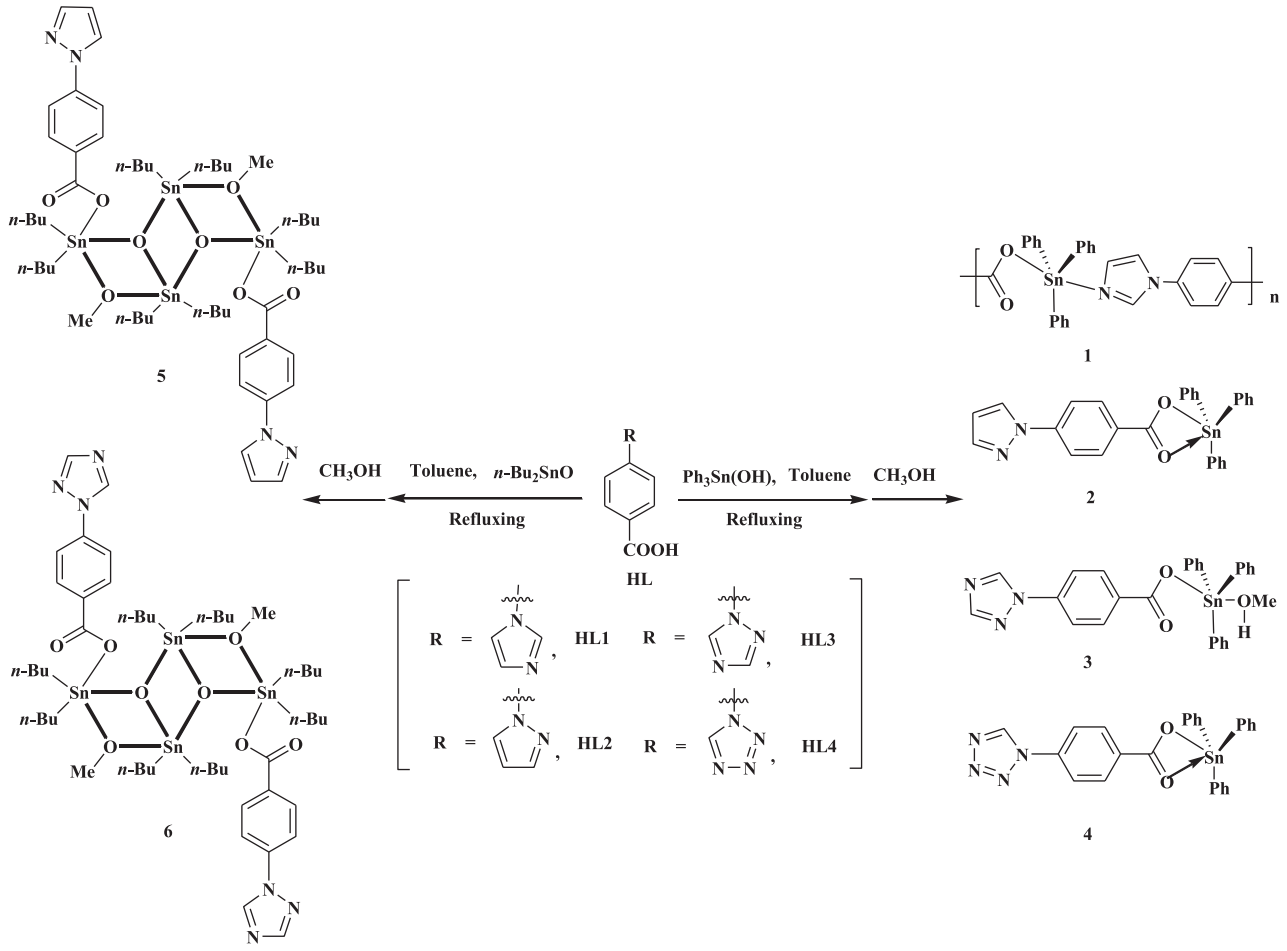


**Scheme 2.** Synthetic route for complexes **1**–**6**.

were recorded with a Nicolet FTIR 170SX instrument using KBr pellets. Elemental analysis was performed with a Perkin-Elmer 240C analyzer. $^1$H NMR spectra were recorded on a Bruker AV 400 spectrometer with tms as internal standard. $^{119}$Sn NMR spectra (proton-decoupled) were recorded on a Bruker AV 400 spectrometer operating at 150 MHz; resonances are referenced to tetramethyltin (external standard, $^{119}$Sn). The luminescent spectra were measured on powder samples at room temperature using a model Perkin-Elmer LS55 fluorescence spectrophotometer. Both the excitation and the emission slits were 10 nm, and the response time was 2 s.

Single-crystal X-ray diffraction measurements were carried out on a Bruker Smart 1000 CCD diffractometer equipped with a graphite crystal monochromator situated in the incident beam for data collection at room temperature. The determinations of unit cell parameters and data collections were performed with Mo K$\alpha$ radiation ($\lambda$ = 0.71073 Å). Unit cell dimensions were obtained with least-squares refinements, and all structures were solved by direct methods with SHELXL-97 [36]. The other non-hydrogen atoms were located in successive difference Fourier syntheses. The final refinement was performed by full-matrix least-squares methods with anisotropic thermal parameters for non-hydrogen atoms on $F^2$. The hydrogen atoms were added theoretically and riding on the concerned atoms.

### 4.2. Synthesis of ligands

See supporting information.

### 4.3. Synthesis of complexes

$Ph_3Sn(OH)$ (370 mg, 1 mmol) and ligands HL1–HL4 (1 mmol) were dissolved in 30 mL toluene and were stirred at 60 °C for 8 h after formed in the reaction was removed by using a Dean–Stark apparatus. The excessive toluene was evaporated and filtered to afford the crude powder. The powder was washed with 5 mL $CH_2Cl_2$ three times and dried in vacuo and then dissolved in 15 mL methanol. Crystals of 1–4 suitable for single-crystal X-ray diffraction analysis were obtained after the solution was allowed to stand for approximately 2 weeks at room temperature, respectively.

Synthesis of **5** and **6** were similar to that of **1**, except that *n*-$Bu_2$SnO (500 mg, 2 mmol) was used instead of $Ph_3Sn(OH)$. Colorless, block crystals of **5** and **6** suitable for single-crystal X-ray diffraction analysis were collected after evaporation at room temperature for about 2 weeks.

*Polymer **1**:* Primrose yellow crystals. Weight: 180 mg, yield: 34%. $^{119}$Sn NMR (DMSO-$d_6$): $\delta$ = −226.374 ppm. *Anal.* Calc. (%) for $C_{28}H_{22}N_2O_2Sn$: C, 62.57; H, 4.10; N, 5.21. Found: C, 62.23; H, 3.97; N, 5.58%. IR (KBr, cm$^{-1}$): 3122 (m), 3066 (m), 1645 (s), 1604 (m), 1514 (s), 1480 (m), 1428 (m), 1309 (s), 1236 (m), 1122 (m), 1061 (s), 782 (m), 733 (s), 698 (s), 451 (m).

*Complex **2**:* Colorless crystals. Weight: 330 mg, yield: 62%. $^{119}$Sn NMR (DMSO-$d_6$): $\delta$ = −107.822 ppm. *Anal.* Calc. (%) for $C_{28}H_{22}N_2O_2Sn$: C, 62.57; H, 4.10; N, 5.21. Found: C, 62.26; H, 3.95; N, 5.54%. IR (KBr, cm$^{-1}$): 3113 (w), 3065 (m), 1622 (s), 1527 (s), 1479 (m), 1606 (s), 1431 (s), 1343 (s), 1200 (s), 931 (s), 857 (s), 733 (s), 988 (s), 696 (s), 589 (s), 447 (s).

*Complex* ***3****:* Primrose yellow crystals. Weight: 400 mg, yield: 74%. $^{119}$Sn NMR (DMSO-$d_6$): $\delta = -111.720$ ppm. *Anal.* Calc. (%) for $C_{28}H_{25}N_3O_3Sn$: C, 58.95; H, 4.39; N, 7.37. Found: C, 58.75; H, 4.23; N, 7.52%. IR (KBr, cm$^{-1}$): 3132 (m), 3049 (m), 1648 (s), 1605 (s), 1518 (s), 1429 (s), 1406 (m), 1327 (s), 1216 (m), 1139 (m), 978 (m), 860 (m), 778 (m), 731 (s), 696 (s), 672 (m), 582 (m), 453 (s).

*Complex* ***4****:* Colorless crystals. Weight: 360 mg, yield: 67%. $^{119}$Sn NMR (DMSO-$d_6$): $\delta = -101.724$ ppm. *Anal.* Calc. (%) for $C_{26}H_{20}N_4O_2Sn$: C, 57.88; H, 3.71; N, 10.39. Found: C, 57.54; H, 3.58; N, 10.61%. IR (KBr, cm$^{-1}$): 3065 (m), 1627 (s), 1507 (m), 1428 (s), 1340 (s), 1215 (s), 1154 (m), 1113 (m), 1073 (s), 988 (s), 858 (s), 776 (s), 734 (s), 697 (s), 587 (s), 447 (s).

*Complex* ***5****:* Colorless crystals. Weight: 320 mg, yield: 48%. $^{119}$Sn NMR (DMSO-$d_6$): $\delta = -146.540$ ppm. *Anal.* Calc. (%) for $C_{54}H_{92}N_4O_8Sn_4$: C, 46.29; H, 6.57; N, 4.00. Found: C, 46.04; H, 6.33; N, 4.29%. IR (KBr, cm$^{-1}$): 3447 (w), 2957 (s), 2927 (s), 2859 (m), 1609 (s), 1551 (s), 1406 (s), 1340 (s), 1044 (m), 934 (m), 855 (m), 783 (s), 748 (s), 622 (s), 486 (s).

*Complex* ***6****:* Colorless crystals. Weight: 250 mg, yield: 37%. $^{119}$Sn NMR (DMSO-$d_6$): $\delta = -138.620$ ppm. *Anal.* Calc. (%) for $C_{52}H_{90}N_6O_8Sn_4$: C, 44.51; H, 6.42; N, 5.99. Found: C, 44.30; H, 6.18; N, 6.35%. IR (KBr, cm$^{-1}$): 3429 (w), 3127 (w), 2957 (s), 2927 (s), 2860 (s), 1607 (s), 1561 (s), 1410 (s), 1347 (s), 1215 (s), 1156 (s), 987 (s), 855 (s), 777 (s), 685 (s), 636 (s), 512 (s).

## Acknowledgments

This work was supported by a grant for the National Natural Science Foundation of China (21071001, 50873001, 20875001), Education committee of Anhui Province (KJ2010A030), Program for New Century Excellent Talents in University (China) The Team for Scientific Innovation Foundation of Anhui Province (2006KJ007TD), Science and Technological Fund of Anhui Province for Outstanding Youth (10040606Y22), The 211 Project of Anhui University, Ministry of Education funded projects focus on returned overseas scholar, Anhui University Student Innovative Experiment Plan (xj103575023, KYXL201100337).

## Appendix A. Supplementary data

CCDC 725513, 719378, 719379, 731652, 748971 and 754610 contain the supplementary crystallographic data for **1**–**6**. These data can be obtained free of charge via http://www.ccdc.cam.ac.uk/conts/retrieving.html, or from the Cambridge Crystallographic Data Centre, 12 Union Road, Cambridge CB2 1EZ, UK; fax: (+44) 1223-336-033; or e-mail: deposit@ccdc.cam.ac.uk. Supplementary data associated with this article can be found, in the online version, at doi:10.1016/j.poly.2011.10.032.

## References

[1] T. Ueno, M. Ohashi, M. Kono, K. Kondo, A. Suzuki, T. Yamane, Y. Watanabe, Inorg. Chem. 43 (2004) 2852.
[2] S. Pal, A.K. Barik, S. Gupta, A. Hazra, S.K. Kar, S.-M. Peng, G.-H. Lee, R.J. Butcher, M.S.E.I. Fallah, J. Ribas, Inorg. Chem. 44 (2005) 3880.
[3] N.-N. Hou, Acta Crystallogr., Sect. E61 (2005) m1197.
[4] S. Shit, S. Sen, S. Mitra, D.L. Hughes, Transition Met. Chem. 34 (2009) 269.
[5] S. Thakurta, J. Chakraborty, G. Rosair, R.J. Butcher, S. Mitra, Inorg. Chim. Acta 362 (2009) 2828.
[6] C. Janiak, Dalton Trans. (2003) 2781.
[7] C. Policar, F. Lambert, M. Cesario, I.M. Badarau, Eur. J. Inorg. Chem. (1999) 2201.
[8] H. Abourahma, B. Moulton, V. Kravtsov, M.J. Zaworotko, J. Am. Chem. Soc. 124 (2002) 9990.
[9] Q.G. Zhai, X.Y. Wu, S.M. Chen, C.Z. Lu, W.B. Yang, Cryst. Growth Des. 6 (2006) 2126.
[10] X.X. Zhao, J.P. Ma, Y.B. Dong, R.Q. Huang, Cryst. Growth Des. 7 (2007) 1058.
[11] V. Chandrasekhar, K. Gopal, P. Sasikumar, R. Thirumoorthi, Coord. Chem. Rev. 249 (2005) 1745.
[12] D.M. Li, R.T. Hu, W. Zhou, P.P. Sun, Y.H. Kan, Y.P. Tian, H.P. Zhou, J.Y. Wu, X.T. Tao, M.H. Jiang, Eur. J. Inorg. Chem. (2009) 2664.
[13] R.R. Holmes, C.G. Schmid, V. Chandrasekhar, R.O. Day, J.M. Holmes, J. Am. Chem. Soc. 109 (1987) 1408.
[14] L.L. Wen, F. Wang, J. Feng, K.L. Lv, C.G. Wang, D.F. Li, Cryst. Growth Des. 9 (2009) 3581.
[15] Z. Zheng, W.Q. Geng, Z.C. Wu, H.P. Zhou, Acta Crystallogr., Sect. E66 (2011) o524.
[16] A. Bondi, J. Phys. Chem. 441 (1964) 441.
[17] F. Caruso', J. Med. Chem. 36 (1993) 1168.
[18] X.Y. Wu, W.L. Kang, D.S. Zhu, C.G. Zhu, S.R. Liu, J. Organomet. Chem. 694 (2009) 2981.
[19] R.G. Swisher, J. Vollanoo, V. Chandrasekhar, R.O. Day, R. Holmes, Inorg. Chem. 23 (1984) 3147.
[20] G.R. Desiraju, Acc. Chem. Res. 29 (1996) 441.
[21] B.G. Zhang, J. Xu, Y.G. Zhao, C.Y. Duan, X. Cao, Q.J. Meng, Dalton Trans. (2006) 1271.
[22] G.R. Desiraju, T. Steiner, The Weak Hydrogen Bond in Structural Chemistry and Biology, Oxford University Press, Oxford, UK, 1999.
[23] T.J. Mooibroek, C.A. Black, P. Gamez, J. Reedijk, Cryst. Growth Des. 8 (2008) 1082.
[24] R. Willem, A. Bouhdid, M. Biesemans, J.C. Martins, D. Vos, E.R.T. Tiekink, M. Gielen, J. Organomet. Chem. 514 (1996) 203.
[25] R. Willem, A. Bouhdid, B. Mahieu, J. Organomet. Chem. 531 (1997) 151.
[26] W.L. Kang, X.Y. Wu, J.B. Huang, J. Organomet. Chem. 694 (2009) 2402.
[27] V. Dokorou, M.A. Demertzis, J.P. Jasinski, D. Kovala-Demertzi, J. Organomet. Chem. 689 (2004) 317.
[28] M.J. Genin, D.A. Allwine, D.J. Anderson, M.R. Barbachyn, D.E. Edward, S.A. Garmon, D.R. Graber, K.C. Grega, J.B. Hester, D.K. Hutchinson, J. Morris, R.J. Reischer, C.W. Ford, G.E. Zurenko, J.C. Hamel, R.D. Schaadt, D. Stapert, B.H. Yagi, J. Med. Chem. 43 (2000) 953.
[29] J. Holecek, M. Nadvornik, K. Handlir, A. Lycka, J. Organomet. Chem. 315 (1986) 299.
[30] C.L. Ma, J.K. Li, R.F. Zhang, D.Q. Wang, J. Organomet. Chem. 691 (2006) 1713.
[31] Y. Liao, J.K. Feng, L. Yang, A.M. Ren, H.X. Zhang, Organometallics 24 (2005) 385.
[32] C. Seward, J. Chan, D. Song, S. Wang, Inorg. Chem. 42 (2003) 1112.
[33] F. Neve, A. Crispini, C.D. Pietro, S. Campagna, Organometallics 21 (2002) 3511.
[34] J.H. Luo, M.C. Hong, R.H. Wang, R. Cao, L. Han, Z.Z. Lin, Eur. J. Inorg. Chem. (2003) 2705.
[35] J. Yang, B. Wu, F.Y. Zhuge, J.J. Liang, C.D. Jia, Y.Y. Wang, N. Tang, X.Y. Yang, Q.Z. Shi, Cryst. Growth Des. 10 (2010) 2331.
[36] G.M. Sheldrick, SHELXL-97, Program for the Refinement of Crystal Structures, University of Göttingen, Göttingen, 1997.